Influence of lithium and lanthanum treatment on TiO$_2$ nanofibers and their application in dye-sensitized and perovskite solar cells

*Filip Ambroz[a], Sanjayan Sathasivam[a], Roxanna Lee[a], Srinivas Gadipelli[a], Chieh-Ting Lin[b,c], Shengda Xun[c], Radhika K. Poduval[d], Martyn Mclachlan[c], Ioannis Papakonstantinou[d], James R. Durrant[b,e], Ivan P. Parkin[a] and Thomas J. Macdonald[*a]*

[a] Department of Chemistry, University College London, 20 Gordon St, London, WC1H 0AJ, United Kingdom

[b] Department of Chemistry, Imperial College London, Imperial College Road, London, SW7 2AZ, United Kingdom

[c] Department of Materials and Centre for Plastic Electronics, Imperial College London, Imperial College Road, London, SW7 2AZ, United Kingdom

[d] Department of Electronic and Electrical Engineering, University College London, Torrington Place, London, WC1E 7JE, United Kingdom

[e] SPECIFIC IKC College of Engineering, Swansea University, Swansea, SA2 7AX, United Kingdom

Abstract

The unique properties of TiO_2 nanofibers (NFs) have generated significant interest in nanostructured photoelectrodes for application in renewable energy. Aside from nanostructuring, the properties of TiO_2 photoelectrodes can be further modified by approaches such as cationic doping, which has been previously used to enhance the performance of the third-generation solar cells. In this study, TiO_2 NFs were produced by electrospinning and modified by introducing lithium and lanthanum cations in one step. X-ray photoelectron spectroscopy and X-ray diffraction analysis showed that the addition of both cations caused minimal substitutional or interstitial doping of TiO_2. Nevertheless, their presence had an influence on crystallite sizes where the introduction of lithium resulted in an increase, whereas lanthanum caused a reduction. The crystal phase of TiO_2 was also affected as lithium promoted the formation of the rutile phase at 500 °C which was detected together with the anatase phase. UV-visible spectroscopy revealed that the lithium modified TiO_2 NFs had a lower band gap energy compared to the control or lanthanum modified TiO_2 NFs. Additionally, Brunauer-Emmett-Teller (BET) measurements showed that lanthanum treated TiO_2 NFs had an increase in the surface area, which even exceeded that of TiO_2 P25 nanoparticles. Finally, treated and un-treated TiO_2 NFs were used for two types of solar cells, namely dye-sensitized solar cells (DSSCs) and perovskite solar cells (PSCs). The photovoltaic measurements revealed that lanthanum treatment was beneficial in both types of solar cells while lithium treatment was found to be detrimental to the device performance for both DSSCs and PSCs.

Introduction

Titanium dioxide (TiO_2) is a widely studied semiconductor material that is stable, non-toxic, inexpensive and has been employed in the field of photocatalysis, such as dye degradation,[1] water splitting,[2] self-cleaning windows,[3] as a battery electrode[4] and as an electron transport layer (ETL) [5] for different types of solar cells. Despite such a wide usage, it possesses particular drawbacks that require modifications of the material. For instance, due to a wide band gap it is only active in the UV region of the solar spectrum which is a significant disadvantage for photocatalysis considering that only 4 % of this high energy light reaches the earth's surface. TiO_2 is commonly found in three different crystal forms, namely metastable anatase (tetragonal), stable rutile (tetragonal) and brookite (orthorhombic) phase.[6] These phases possess different characteristics, where the most suitable one for solar cell applications is the anatase phase due to its superior charge transport ability.[7]

Spherical nanoparticles (NPs) are the most common morphology used for metal oxide-based photoelectrodes in photovoltaics. However, morphologies such as one-dimensional (1D) nanostructures are promising alternatives where unique properties such as directionality and decreased grain boundaries

have been shown to be beneficial for device performance.[8,9] In particular, the electron transport rate in 1D TiO$_2$ nanofibers (NFs) is significantly faster when compared to NPs since the grain boundary scattering of free electrons is substantially reduced.[10] Despite these benefits, NFs suffer from low surface area which is disadvantageous in the field of solar cells, particularly for DSSCs where it leads to low dye uptake. While the addition of NPs has been reported to circumvent such limitations in NF-based photoelectrodes,[11] doping TiO$_2$ with cations and anions has been previously used in particulate-based systems to modify the electronic properties of TiO$_2$.[7] Since the type of dopants will have different influence on a material's characteristics, they should be selected based on the alterations that are required to be achieved. In the case of TiO$_2$, substitutional doping can be achieved by either replacing cations (Ti^{4+}) or anions (O^{2-}) with other metals and non-metals, respectively. In this framework, many studies have been performed where researchers used various types of cationic dopants to modify the characteristics of TiO$_2$ to improve the performance of the related applications.[7] For instance, to improve the photocatalytic activity of TiO$_2$, lanthanum (La) compounds were previously used and shown to be advantageous in improving photocatalytic dye degradation.[12] It has been shown that doping TiO$_2$ with La^{3+} ions improves the rate of the adsorption of the organic compounds which is associated with the formation of oxygen vacancies.[13] When La^{3+} ions are introduced to TiO$_2$ they scavenge oxygen to form La – O bonds that have a stronger chemical bonding energy in comparison to Ti – O bonds. As a result, oxygen vacancies form which has an influence on the level of dye adsorption and charge transport within the material.[13] The increased level of dye uptake is particularly favorable for the photovoltaic performance of dye-sensitized solar cells (DSSCs). In addition, lithium (Li) doping of TiO$_2$ has been shown to have similar influence as it increases conductivity and charge densities.[7] The introduction of Li^{2+} ions lowers the conduction band edge of TiO$_2$ which improves electron injection and transport.[5] All previous studies were only carried out in nanoparticulate systems of TiO$_2$, the influence of such cationic treatments for other morphologies such as TiO$_2$ NFs are yet to be studied. Since morphology alternations can result in modified electronic and physical properties, it is important to study the effect of introducing common dopants to understand any beneficial or detrimental effects.

Recently, perovskite solar cells (PSCs) have opened new research avenues for efficient and cheap solar energy generation. While the field is rapidly moving forward, a majority of the work focuses on nanoparticulate ETLs, whereas only a minority have investigated TiO$_2$ NFs as a mesoporous layer. Boix et al.[14] firstly reported TiO$_2$ NF PSCs where NFs were directly electrospun atop a compact TiO$_2$ layer. This was followed by the report of Wu et al.[15] where they doped TiO$_2$ NFs with lead and the study of Hong et al.[16] where they used gold as a dopant element. Batmunkh et al.[17] later made a composite TiO$_2$-carbon nanotube (CNT) photoelectrode, where the CNTs were found to provide a significant boost in performance enhancement, also justified by previous reports.[18] On the other hand, Li doping of nanoparticulate TiO$_2$ in perovskite solar cells (PSCs) has been reported to enable faster electron transport by reducing electronic

trap states.[5] Despite this breakthrough, the effects of lithium or lanthanum doping are yet to be studied on TiO_2 NFs.

In this study, TiO_2 NFs were produced *via* electrospinning and modified with La and Li salts that were both separately added directly in the precursor sol-gel solution. The influence of TiO_2 NF modification was investigated by XPS, XRD, UV/Vis and Raman and the surface area and porosity changes were analyzed using the BET method. Microscopy techniques were also employed, for instance SEM, TEM and SAED to monitor any morphological changes. Finally, TiO_2 NFs were employed for two types of solar devices, namely for DSSCs and PSCs. In the former type they were used as a light scattering layer while in the PSC cell configuration they were employed as a mesoporous layer. This work is the first example where La and Li modified TiO_2 NFs were used for such an application. We describe a simple route to produce and modify TiO_2 NFs in one step and explore how the addition of La and Li metal salts affects the crystal structure of TiO_2 together with the influence it has on the performance of the solar cells.

Experimental Section

Materials

All chemicals used in this study were purchased from Sigma Aldrich (UK) unless otherwise stated. They were used without further purification.

Preparation of TiO_2 precursor solutions

TiO_2 NFs were prepared following reports of our previous study.[19] Briefly, a sol-gel solution was prepared by dissolving 0.5 g of poly(vinyl pyrrolidone) (PVP, M=1 300 000) in absolute ethanol (5 mL) followed by stirring for 24 h. Subsequently, titanium (IV) butoxide (2.5 mL) was added drop-wise. It should be noted that if PVP is not properly dissolved in ethanol, upon the addition of titanium (IV) butoxide a white precipitate solution forms which cannot be used for the process of electrospinning. After titanium (IV) butoxide was added, the resulting solution was stirred for 24 hours. For the preparation of Li-doped TiO_2 precursor solution, 1 mol% of Li acetate (99+% anhydrous) was added after PVP was completely dissolved in ethanol (24 h) followed by the additional 24 h stirring. Afterwards, titanium (IV) butoxide (2.5 mL) was added drop-wise. La-doped TiO_2 precursor solution was prepared by first dissolving PVP in 4 mL of ethanol. In a separate vial, La(III) chloride hepta-hydrate (99.999% trace metals basis) was dissolved in 1 mL of ethanol by sonication. Subsequently, this solution was added drop-wise to the vial with dissolved PVP and left for 24 h stirring before the addition of titanium (IV) butoxide (2.5 mL).

Preparation of TiO_2 NFs

The TiO_2 sol-gels were electrospun at a voltage of 10 kV with a flow rate of 1 mL h^{-1}. During this process the distance between the collector plate and the needle tip was kept constant (10 cm) to ensure nanofiber formation remained consistent. The resulting NF mats were subject to pyrolysis at 500 °C for 12 h ensuring that PVP was completely removed.

Preparation of TiO$_2$ NF DSSCs

Three different types of NFs (0.25 g each) were separately mixed with ethanol (20 mL) following by sonication for at least 2 h until no solid traces of NFs could be seen. Sonication may take longer than 2 h depending on sonication power, the most important thing is that no solid NFs remain. Once a uniform solution was achieved, 1 mL of terpineol was added and further sonicated for 15 min. Ethanol was removed by rotary evaporation for approximately 30 min resulting in a white paste. To prepare photoanodes, fluorine-doped tin oxide (FTO) glass was cleaned with water solution of teepol followed by Milli-Q water, acetone and ethanol with 10 min of sonication each. Transparent TiO_2 photoanodes were prepared by doctor blading commercially available TiO_2 paste (GreatCell Solar, DSL-18NRT) onto FTO glass. Such photoanodes were sintered at 500 °C resulting in a uniform transparent TiO_2 NPs anatase layer. The transparent photoelectrodes were subject to treatment with an aqueous solution of titanium tetrachloride (or titanium (IV) chloride) ($TiCl_4$, 40 mM) for 30 min at 70 °C. After treatment, the photoelectroodes were washed with Milli-Q water and sintered at 500 °C. It is noteworthy that the active solar cell area of our photoelectrodes was 0.1256 cm^2. Directly after sintering the temperature was decreased to 80 °C and the photoelectrodes underwent dye sensitization with a solution of ruthenizer 535-bisTBA (Solaronix 0.5 mM) in absolute ethanol for 20 h in the dark. The photoelectrodes were subsequently carefully washed with ethanol to remove un-anchored dye molecules from the surface. As counter electrode Pt-coated FTO glass (GreatCell Solar) was used. Sensitized photoelectrodes were eclipsed with counter electrodes with a thermoplastic sealant (GreatCell Solar, MS004610) following by heating at 100 °C for 11 min to seal the sealant. A redox mediator consisting of iodine (I_2 0.05 M), 1.2-dimethyl-3-propylimidazolium iodide (DMPII 0.6 M), guanidinium thiocyanate (0.10 M) and 4-tert-Butylpyridine (TBP 0.5 M) in a mixture of acetonitrile and valeronitrile (volume ratio, 85:15) was injected into the sealed electrodes by vacuum filling.

Preparation of TiO$_2$ NF PSCs

Firstly, FTO was etched using 2M HCl and zinc metal, followed by sequential cleaning in detergent, deionized water, acetone, ethanol, and isopropanol. As a final cleaning step, the FTO was treated with oxygen plasma for 10 min. A thin compact layer of TiO_2 (cp-TiO_2) was then deposited onto the FTO by spin coating a solution of 0.1M titanium diisopropoxide bis(acetylacetonate) (75 wt% in isopropanol), in 1-butanol at 3000 rpm for 20 s. After spin coating, the substrates were immediately heated at 150 °C for 2 min. This process was done in air and repeated twice to ensure a dense blocking layer was formed without pinholes. The cp-TiO_2 layer was then heated to 500 °C at a ramp rate of 50 °C min^{-1} and left at 500 °C for 25 min. Untreated, Li and La treated TiO_2 NFs were then made into a paste by making a solution of 30 mg mL^{-1} in ethanol and sonicating until no solid NFs remained (~ 2 h) followed by the addition of terpineol (4.9 g of terpineol per 1 g of NFs). The solution then underwent an additional 30 min of sonication. Each NF solution was then spin coated at 4000 rpm for 30 s on top of the cp-TiO_2 forming a NF scaffold. The substrates were then heated to 500 °C at a ramp rate of 50 °C min^{-1} and left at 500 °C for 25 min. The substrates were then transferred to a nitrogen filled glovebox ready for perovskite deposition. The perovskite solution was prepared with slight modification to procedure previously reported in the literature by Ahn et al.[20] Briefly, the $CH_3NH_3I \bullet PbI_2 \bullet DMSO$ adduct solution was prepared by mixing 461 mg of PbI_2 and 159 mg of CH_3NH_3I with 600 mg of DMF and 78 mg of DMSO. The solution was stirred in a nitrogen filled glovebox for 1 h at 65 °C and filtered before use. The filtered solution was spin coated on the previously prepared TiO_2 films at 5000 rpm for 30 s and after 7 s had elapsed, 0.5 mL of diethyl ether was slowly dripped onto the rotating substrate. The transparent $CH_3NH_3I \bullet PbI_2 \bullet DMSO$ adduct film was heated to 65 °C for 2 min and 100 °C for 10 min to obtain a dense $CH_3NH_3PbI_3$ film. For the hole transport material (HTM), a 10 mg mL^{-1} solution of PTAA in toluene was prepared by stirring in a nitrogen filled glovebox for 1 h at 65 °C. The fully dissolved solution was then doped with additives of 7.5 μL bis(trifluoromethane)sulfonimide lithium salt (Li-TFSI)/acetonitrile (170 mg mL^{-1}) and 4 μL of 4-tert-butylpyridine (tBP). Finally, 65 nm of Au was thermally evaporated as a counter electrode.

Materials Chemistry and Characterization

All details can be found in the Supporting Information.

Results and Discussion

Our previous work has established effective techniques to produce gold NPs (AuNP) and CNT modified TiO$_2$ NFs that can be utilized for PECs.[18,19] However, the method of preparing such nanomaterials requires two steps since AuNPs and CNTs are separately added to already formed TiO$_2$ NFs which is less convenient and can be associated with increased production costs. In this work we directly added Li and La salts to the TiO$_2$ sol-gel precursor solution for electrospinning, to produce both treated and untreated TiO$_2$ NFs in one step. Such a facile, single-step electrospinning approach can be cost effective and therefore more industrially friendly.

Scanning Electron Microscopy (SEM) was performed to visualize the surface topography and determine if the structure of the TiO$_2$ NFs has been affected by the addition of metal salts. SEM images of electrospun La and Li modified TiO$_2$ NFs after the calcination step (500 °C) can be seen in Figure 1a and b. SEM images of control TiO$_2$ NFs are shown in Figure S1 in the Supporting Information (SI). The NFs exhibit an interweaving network with different length sizes up to several tens of micrometres without any significant defects on their surface. Compared to the control TiO$_2$ NFs, no difference in morphology was observed upon the addition of La or Li. While the morphology of the NFs was consistent with and without Li and La treatment, breakages (as observed in Figure 1) in the fibers is commonplace and can be attributed to the calcination treatment.[21] Breakages from calcination are due to the polymer coating removal at high temperatures which causes NFs to break into lengths that are influenced by the bonding in the polymer which is expected to be relatively uniform along the polymer chain. The calcination also results in a denser product. The diameter of our NFs was determined to be over 120 nm without any noticeable change or trends upon the addition of metal salts.

To further investigate if La or Li metal salts have induced any structural changes of TiO$_2$ NFs, transmission electron microscopy (TEM) was used to image a single NF of each type. Figure 1c and d show a high-resolution (HR) images of an isolated La and Li modified TiO$_2$ NFs. (See Figure S1c for control TiO$_2$ NF) The images reveal that NFs consisted of a large number of NPs that build up a 1D nanomaterial. Despite the use of HR-TEM, traces of La or Li metal oxides were not visible in our images which we attribute to the low concentration present (1 mol%). Further characterization with HR-TEM revealed that the metal salt modifications did not induce any changes in the inter planar spacing as it was measured to be 0.32 nm corresponding to the (101) plane of the anatase TiO$_2$ (Insets of Figure 1c and d for La and Li modified and Figure S1c for control TiO$_2$ NFs). All types of NFs exhibit well crystallized areas of TiO$_2$ having a similar outline. No La$_2$O$_3$ was observed for the La modified TiO$_2$ NFs (Figure 1c) or Li oxides for the Li modified TiO$_2$ NFs (Figure 1d). The Selected-area electron diffraction (SAED) pattern of our NFs consisted of bright spots which are a result of the diffraction from a single crystal confirming their good crystallinity (Figure S1d). Moreover, the *d*-spacing values were matched with the formation of the anatase phase corresponding with the XRD results.
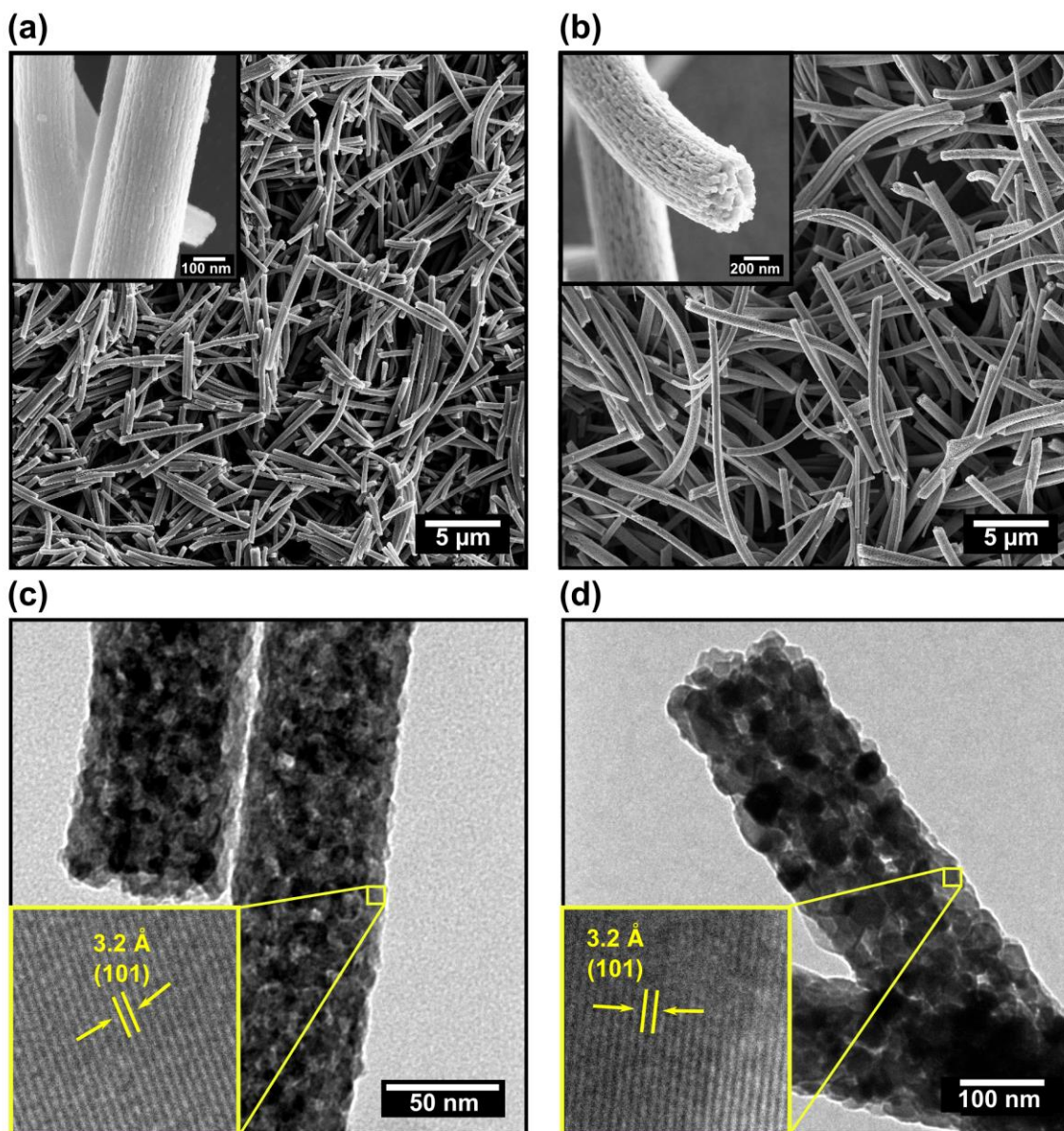
Figure 1. (a) And (b) show top-view SEM images of La and Li modified TiO_2 NFs with insets of their high-resolution images. (c) And (d) shows TEM images of a single isolated La and Li modified TiO_2 NFs with lattice planes as insets confirming high crystallinity.

Since electron microscopy does not indicate the presence of La or Li in the TiO_2 lattice, X-ray photoelectron spectroscopy (XPS) was used to verify the elemental components of the synthesized TiO_2 NFs. Figure S2 illustrates the XPS spectrum for the Ti 2p transition of the control TiO_2 NFs. It shows the typical two spin-orbit components with the Ti $2p_{3/2}$ peak centred at 458.4 eV and Ti $2p_{1/2}$ peak located at 464.1 eV

corresponding to Ti in the +4 oxidation state. For the La and Li modified TiO_2 NFs the Ti $2p_{3/2}$ peak appears at the same position of 458.4 eV respectively, also matching Ti^{4+} (Figure S2). For the all three samples, no additional peaks were observed corresponding to any Ti^{3+} surface states which is in agreement with the report of Giordano et al.[5] for their control and Li modified samples. However, in the same work they reported the interaction between Li and O based on the O 1s spectra that could indicate the formation of oxygen vacancies. It should be noted that the conclusions based on the O 1s spectra can be debatable as it takes meticulous sample preparation and handing to avoid oxygen contamination. While our comparison of the O 1s spectra for the modified TiO_2 NFs could suggest possible interactions, the conclusions were regarded as inconclusive since Li or La could also interact with the O from the environment.

For the La modified TiO_2 NFs, La was successfully detected by XPS as shown in Figure 2a. The La 3d spectrum is made up of the 3d component and associated satellite peaks. The main La$3d_{5/2}$ transition of the doublet is centred at 834.6 eV and La$3d_{3/2}$ at 851.4 eV corresponding to the literature values of La in the +3 oxidation state. The XPS results suggest that the La is in the form of La_2O_3 dispersed on the TiO_2 NFs with minimal substitutional or interstitial doping of TiO_2. Evidence for this is provided by XRD data (see Figure 3a) where a lack of TiO_2 unit cell expansion was observed compared to the control TiO_2 sample as well as the literature standards.[22] Due to the large ionic radius of La^{3+} (0.103 nm) compared to Ti^{4+} (0.061 nm), doping would cause the tetragonal unit cell of TiO_2 to expand resulting in a shift in the XRD peaks to lower 2Θ values compared to the control which was not seen for our samples. XPS was also successful in detecting Li on the surface of the Li modified TiO_2 NFs. A weak but distinct signal for Li 1s can be seen between 57 and 53 eV that was not present in the control sample where only noise was observed as illustrated in Figure 2b. Due to Li being a very light element, it is notoriously difficult to detect it with X-ray based techniques since it shows little to no sensitivity to such measurements. However, comparing to other studies in the literature,[5] our signal can be considered as substantial, undoubtedly showing that Li was present in our material (inset Figure 2b).
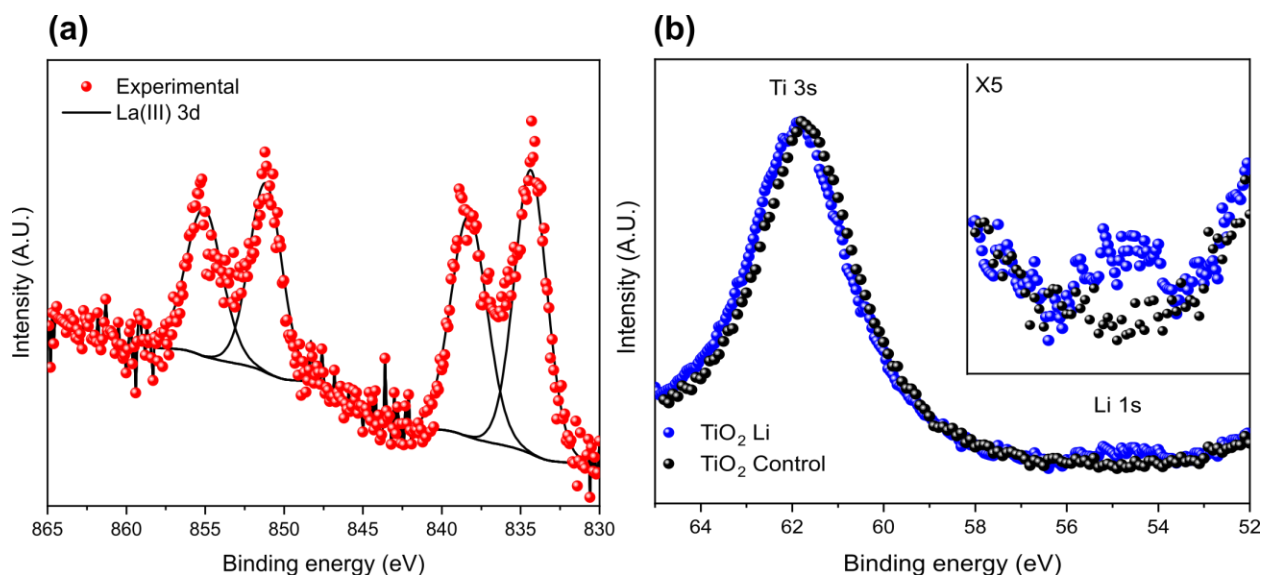
Figure 2. X-ray photoelectron spectroscopy (XPS) for La (a) and Li (b) modified TiO_2 NFs. The inset shows the range between 48 and 58 eV confirming the presence of Li. All peaks were fitted using CasaXPS software.

X-ray diffraction (XRD) was used to evaluate how different metal salts affect the crystal phase of TiO_2. The XRD patterns of control, La and Li modified TiO_2 NFs are shown in Figure 3a. It can be seen that all the samples exhibit signals of the anatase phase which is the most suitable for solar cells.[7] The XRD pattern of La modified TiO_2 NFs shows that La had an influence on the crystallinity since the peaks are not as well-defined compared to the XRD patterns of control and Li modified TiO_2 NFs indicating that the material was less crystalline. As observed by XPS, La_2O_3 was present in La modified TiO_2 NFs, however its crystalline phase was not detected by XRD since the amount of La salt added was very low (1 mol%). Based on the positions of the XRD peaks for control and La modified TiO_2 NFs no shifts or crystal lattice distortion have been observed, indicating that La^{3+} did not seemingly enter into the crystal lattice of TiO_2 to substitute for Ti^{4+}. This was further verified with almost identical lattice volumes (Table S1 – the difference is within error) suggesting that no incorporation of La ions into the bulk lattice occurred. The Scherrer equation was employed to obtain crystallite sizes from (011) and (020) anatase planes positioned at 11.37 and 21.71 2Ө degrees of the XRD spectra. Our results showed that the size compared to the control TiO_2 NFs decreased after La modification by 43 %. Since La^{3+} ions did not enter into the TiO_2 lattice their presence between the crystallites likely caused grain boundary defects which can hinder crystal growth.[23] On the other hand, the size of the crystallites after Li modification increased by only 16 %. The position of the anatase peaks for Li modified TiO_2 NFs also remained the same compared to the control suggesting that no structural rearrangement occurred upon Li modification. Based on the XRD pattern for Li modified TiO_2 NFs, additional peaks that cannot be seen for control and La modified TiO_2 NFs appeared. These new peaks

10

matched the rutile phase of TiO_2. Since all NFs were sintered at 500 °C, it is evident that the addition of Li salts to the precursor solution facilitated the formation of the rutile phase that normally occurs between 600 - 800 °C. It can also be noted that compared to La modification, the diffraction peaks are narrower and better defined which is a characteristic of higher crystallinity. Lattice parameters and volumes were also measured for Li modified TiO_2 NFs (Table S1), however no difference was observed comparing to the control sample indicating that Li ions did not enter into the lattice of TiO_2. Another important feature of the XRD patterns in Figure 3a is that all the signals for the anatase phase shifted to lower 2Ө values compared to the standard diffractogram which is an indication of a unit cell expansion. Since this phenomenon was observed for all types of TiO_2 NFs, we attribute it to the nanostructuring of the materials.

To evaluate how the addition of metal salts affect the light scattering characteristics of our materials, Raman spectroscopy was performed. Figure 3b shows the Raman spectra for control, La and Li modified TiO_2 NFs. The Raman shift for control TiO_2 NFs are located at 142.4, 195.1, 394.7, 515.6, and 637.6 cm^{-1} and correspond to E_{1g}, E_{2g}, A_{1g}, B_1, and E_{3g} vibration modes of the anatase phase of TiO_2.[19] While the same phase can also be identified for La modified TiO_2 NFs, a slight shift can be observed for the main anatase vibration mode E_{1g} (143.5 cm^{-1}) and B_1 (517.7 cm^{-1}) while the shift for vibration mode A_{1g} (398.8 cm^{-1}) is more pronounced. As reported by other researchers in the field[23] the shift for symmetry E_{1g} indicates different crystallite sizes. Particularly, the shift to higher wavenumbers is related to the reduction in crystallite sizes which is in agreement with our XRD results where it was estimated using the Scherrer equation that La reduced crystallite sizes. The size reduction also results in more broadened peak (E_{1g} vibration modes) which is illustrated in the inset of Figure 3b.[24] Furthermore, it was reported that the shift of the E_{1g} vibration modes is related to the rise of oxygen vacancies.[23] Since such phenomenon can be observed in the Raman spectra for La modified TiO_2 NFs (Figure 3b), this provides evidence for the formation of oxygen vacancies. The Raman spectra for Li modified TiO_2 NFs showed a similar pattern compared to the control and La modified TiO_2 NFs. On the other hand, the XRD pattern for the Li modified TiO_2 NFs revealed the presence of the rutile phase. The latter phase can also be detected by Raman spectra where a weak but distinct signal for E_g vibrational modes at 445.3 cm^{-1} can be observed and is illustrated together with the control TiO_2 NFs in Figure S3.

UV/Vis spectroscopic studies were performed to monitor if the addition of metal salts induced any band gap changes in the TiO_2 NFs. Figure 3c illustrates the Tauc plots that was obtained based on the UV/Vis absorption measurements of the TiO_2 NF films where the band gap values are given in Table S2. Using this approximation method, it was determined that the band gap of the control and La modified TiO_2 NFs is 3.08 eV and 3.07 eV, respectively. Such a small change is within error, however since the crystallite sizes decreased upon La modification the blue shift can also be attributed to the photon confinement effect.[23] On

the other hand, the band gap for the Li modified TiO_2 NFs was determined to be 2.92 eV which is noticeably lower meaning that the Li modification was clearly responsible for the red shift. As the rutile phase of TiO_2 has a lower band gap compared to the anatase phase, such decrease is related with the presence of the latter phase which was detected for Li modified TiO_2 NFs *via* XRD and Raman spectroscopy. It is noteworthy that the same measurements were also performed for the powders of TiO_2 NFs, however comparing to the films no significant difference in the band gap values were observed (Table S2).
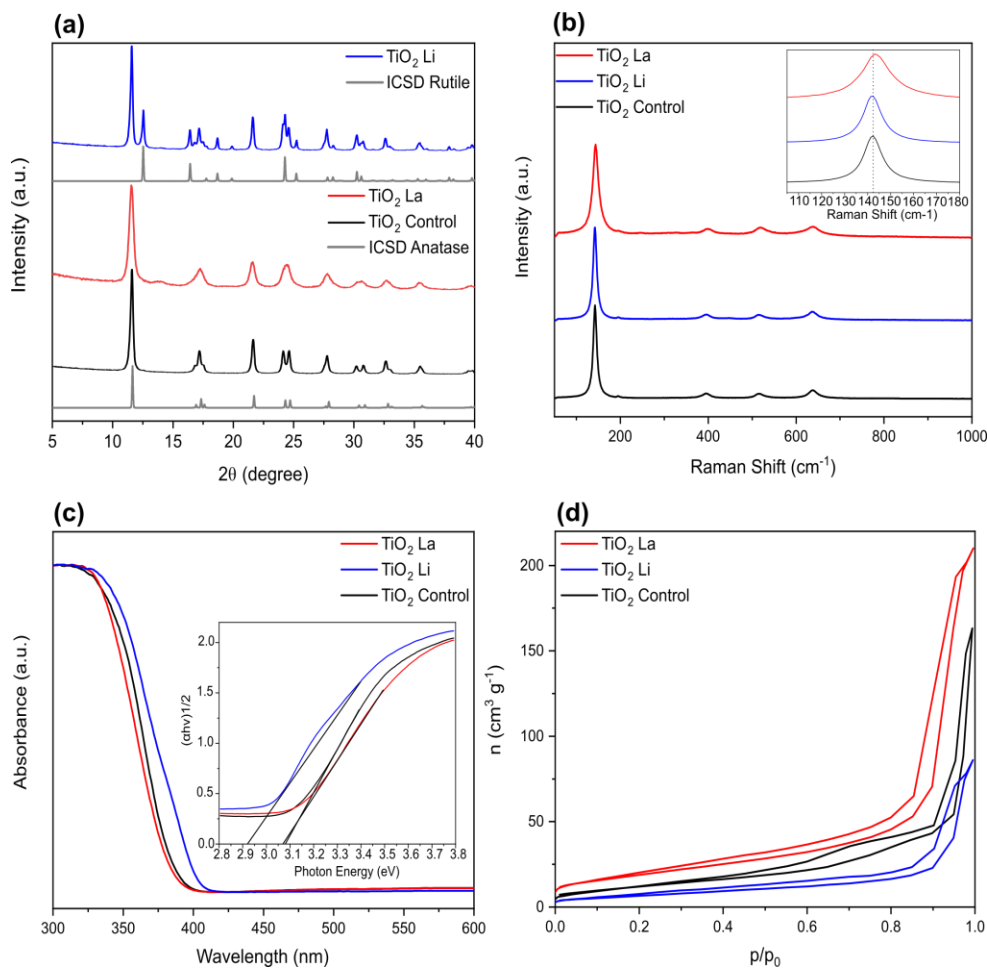

Figure 3. (a) Shows the X-ray diffraction (XRD) spectra for control, La and Li modified TiO_2 NFs confirming the presence of the anatase and rutile (Li modification) crystal structures. (b) Shows the Raman surface scan for control, Li and La modified TiO_2 NFs. The inset shows a slight shift for the main anatase vibration mode E_{g1} (143.47 cm^{-1}) to higher wavenumbers. (c) Shows the UV-Visible (UV-Vis) absorption spectroscopy where the inset shows the Tauc plot confirming the band gap of TiO_2 NFs. (d) Shows N_2 adsorption isotherms obtained for control, Li and La modified TiO_2 NFs; n: amount of N_2 adsorbed at standard temperature and pressure (STP).

One of the main drawbacks of 1D nanomaterials for their use in solar cells is their low surface area. To circumvent such unfavourable characteristics, a very popular approach is doping since it has been reported that the modifications with particular metals can increase the BET surface area.[7] To investigate how the La and Li modifications affected the BET surface area of our TiO_2 NFs, N_2 gas adsorption measurements were performed and the results are shown in Table 1. Figure 3d shows the physisorption isotherms that were used for the determination of the BET surface area and porosity.[25] For comparison, P25 TiO_2 NPs were also included. As expected, P25 NPs had a 27.6 % higher BET surface area compared to the control TiO_2 NFs where the porosity difference was even higher (54.3 %). However, the highest BET surface area was achieved for the La modified TiO_2 NFs where it increased by 34.8 %. Remarkably, such an increase resulted in a value that was even higher than P25 NPs despite the porosity being noticeably lower. On the other hand, Li modification had the opposite effect since the BET surface area decreased by 45.2 % comparing to the control TiO_2 NFs and was therefore for almost 3-fold lower than for the La modified TiO_2 NFs. The porosity decrease was even greater since it reduced almost by a factor of 19 against the control and for more than 24 times comparing to the La modified TiO_2 NFs. Considering the trends obtained from the XRD measurements where La modification reduced crystallite sizes as opposed to Li modification where they increased, such trends in the BET surface areas were also anticipated.

Table 1. The BET surface area and porosity for control, La and Li modified TiO_2 NFs together with the values for P25 NPs.

Sample	BET (m^2 g^{-1})	Porosity (cm^3 g^{-1})
Control	45.6	0.252
La modification	70.0	0.325
Li modification	25.0	0.0133
P25	63.0	0.551

To evaluate the photovoltaic characteristics of the TiO_2 NFs, DSSCs and PSCs were fabricated and measured under AM 1.5 simulated sunlight. A cross-sectional SEM image of the DSSC photoelectrode configuration is shown in Figure 4a. It consists of two main layers, namely a transparent layer of TiO_2 NPs and a light-scattering layer of TiO_2 NFs. The thicknesses of both layers were determined to be approximately 8 µm and 4 µm, respectively which aligns well with the optimum film thickness to produce efficient DSSCs.[19] On the other hand, a PSC device cross-section is illustrated in Figure 4b where it consist of more layers, such as a blocking layer of TiO_2 NPs, a TiO_2 NF based mesoporous layer, a perovskite layer

of methyl ammonium lead iodide (MAPI), a layer of hole-transport material, specifically poly(triaryl amine) (PTAA) and a layer of a metal contact (Au).
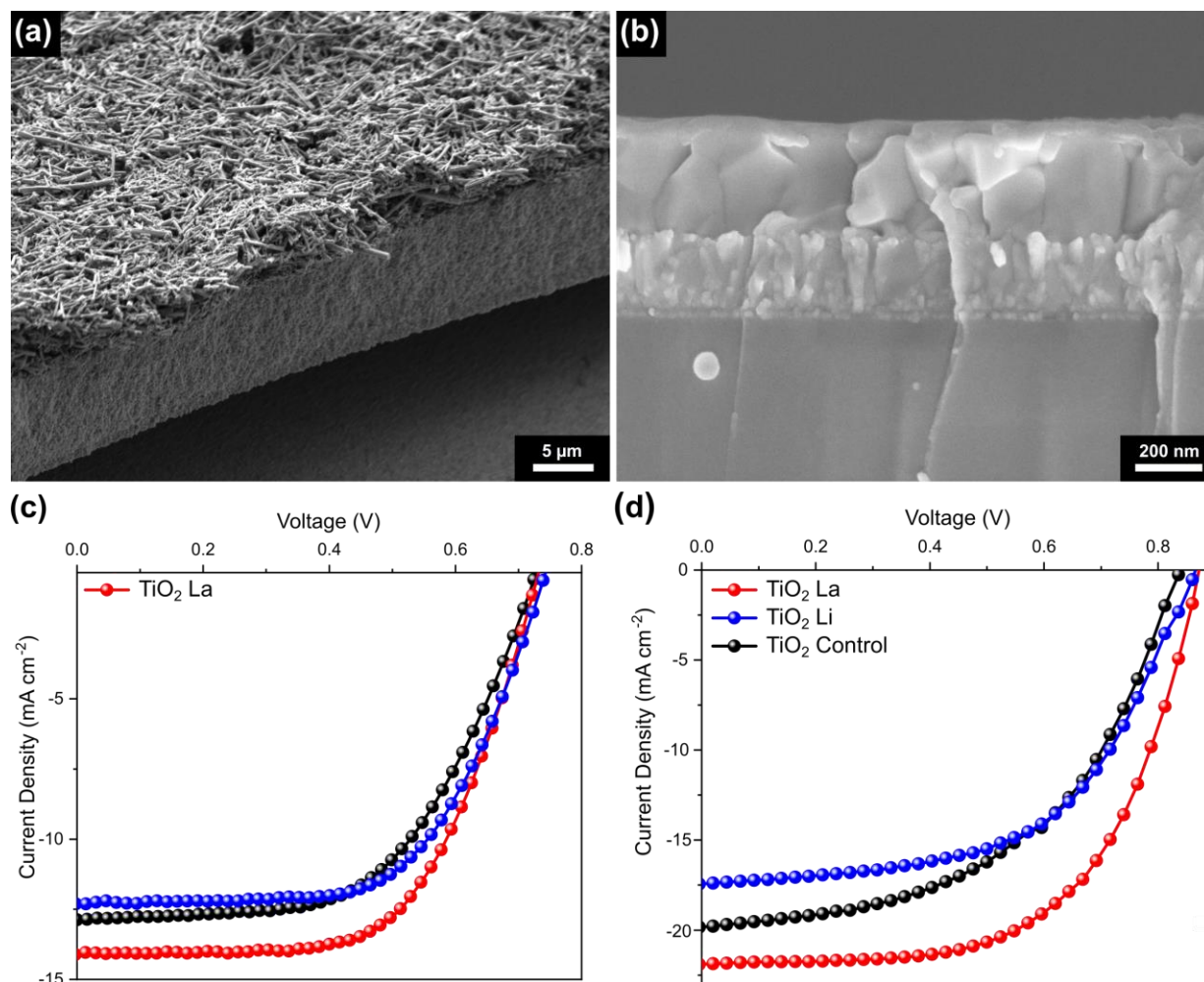

Figure 4. Cross-sectional SEM image of a DSSC (a) and a PSC (b) device configuration. J-V characteristics of DSSCs (c) and PSCs (d) containing control, Li and La modified TiO_2 NFs. The measurements were performed under 1.5 AM conditions where a silicon reference cell was used for the calibration.

Figure 4c shows the J-V curves of the highest performing control, La and Li modified TiO_2 NF based devices. Their photovoltaic properties are summarized in Table 2. It is noteworthy, that the average values of the photovoltaic parameters for different batches of devices are presented in Table S3 where the trends were identical as discussed herein. As illustrated, the highest performing device was obtained with La modified TiO_2 NFs where an overall conversion efficiency increased by 17.2 % compared to the control device. Such an improvement can mostly be attributed to an increase in a short-circuit current density (J_{SC}) (~9 % improvement) and fill factor (FF) (~8 % improvement), respectively. Furthermore, as indicated by

the BET measurements, La modification resulted in the highest surface area which can influence dye adsorption and lead to an improvement in performance. Treated and un-treated TiO_2 NF photoelectrodes were used to determine the amount of adsorbed dye by performing dye-desorption experiments (Table S4). The highest dye absorption occurred for the material that had the highest BET surface area, the La modified TiO_2 NFs. While the latter material consisted of oxygen vacancies as confirmed by Raman spectroscopy which improves dye uptake,[13] we believe that the main reason for the increase was high BET surface area. On the other hand, the Li modified TiO_2 NFs exhibited the lowest BET surface area, however their dye uptake was in the same range as for the control TiO_2 NFs. It should be noted that such a small difference between them can be attributed to the experimental error. therefore we cannot corroborate which type had a higher amount of adsorbed dye. Since the dye adsorption is often related with DSSCs device performance where higher dye uptake is associated with higher J_{sc} our dye desorption tests (Table S4) follow the trends in Table 2. While for the La modified TiO_2 devices J_{sc} increased comparing to the control devices, the same trend was not observed for the Li modified TiO_2 devices as they exhibit lower values, in the range similar to control DSSCs. However, their overall power conversion efficiency (PCE) was slightly higher comparing to control which was a result of higher open-circuit voltage (V_{OC}) (<14 mV) and FF (~8 % improvement). As discussed earlier, based on the XRD results Li modification promoted the formation of the rutile phase that was detected together with the anatase phase. Since these two TiO_2 phases have different band structures, high proportion of the rutile phase is not desirable for solar cells as a result of the increased charge recombination. As photovoltaic parameters in Table 2 show, the addition of Li salts did not have a beneficial effect on the J_{sc} values. Moreover, J_{sc} was even slightly lower comparing to the control DSSCs. As reported by Wang et al.[26], Li-doping is only beneficial for DSSCs with small sized NPs (6 nm) while large particle sizes decrease device efficiencies. For small sized NPs Li ions are highly reversible since they are inserted into the layers on the surface as opposed to bigger NPs where Li ions are inserted into the bulk, consequently they become gradually trapped.[26] Therefore, charge transport will be influenced by different Li insertions. Our photovoltaic parameters indicate that the Li modified TiO_2 NFs did not result in Li insertions that would promote charge transport. For the La modified TiO_2 NFs V_{OC} was relatively similar to the control DSSCs while Li modification was proved to increase it notably. It was suggested that such an increase initiated by a dopant can be attributed to a negative shift of V_{FB} which increases E_F and CB.[7] The FF increased for both modified devices. Such finding is in agreement with the reports of other researchers in the field,[13,26] however to gain further understanding, the average resistance measurements for different devices were compiled in Table S5 with additional discussion in the supporting information..

Table 2. Photovoltaic parameters for the highest performing DSSC devices.

Device	J_{SC} (mA cm^{-2})	V_{OC} (mV)	FF (%)	PCE (%)
Control	12.8	735	56.8	5.3
La modified	14.1	737.5	61.6	6.4
Li modified	12.3	749.4	61.3	5.6

Furthermore, to evaluate how our TiO$_2$ NFs perform in a thin-film configuration with a strong light absorbing material instead of a photoactive dye, PSCs were fabricated, and J-V curves are illustrated in Figure 4d. The average photovoltaic performance of separate batch of devices is shown in Table S5 with the same trends as for the PSCs discussed herein.

Table 3 shows the solar cell parameters extracted from the J-V curves in Figure 4d. It should be noted that to obtain a uniform layer of TiO$_2$ NFs which was suitable for a device fabrication, an optimization of the NF concentration and spin coating parameters were required. Figure S4 demonstrates how the parameters affected the coverage of the TiO$_2$ NFs where Figure S5 shows the coverage that was obtained using the parameters for the deposition of a mesoporous layer for our PSCs. Compared to DSSCs photovoltaic data, the same trends were also observed for PSCs where the best devices were obtained for La modified TiO$_2$ NFs. While J_{SC} for a control PSC (19.8 mA cm^{-2}) was already higher compared to the champion DSSC, it increased even further after La modification to the value of 21.9 mA cm^{-2}. We attribute the increase to the improved charge transport as a result of oxygen vacancies that hindered charge recombination of electrons and holes by trapping electrons through the NF layer.[27] Moreover, such material's defects can also reduce the accumulation of injected electrons from the perovskite layer to the electron transport layer (ETL) which improves the level of charge recombination. As the electrons are trapped in oxygen vacancies the amount of free electrons in the material increases which has influence on its conductivity.[27] Therefore, such vacancies could also be considered as *n*-type dopants. La modification also improved V_{OC} as it increased on average for 49.7 mV (Table S6). While such an increase was not observed for DSSCs, La modified PSCs exhibited the highest values among all which can be attributed to the Fermi energy tuning that has an influence on the device's photovoltage. On the other hand, the enhancement of FF can be associated with the series and shunt resistances (Table S7).

The combination of improved J_{SC}, V_{OC} and FF for the La modified PSC resulted in the highest PCE of 11.5 %. As opposed to La, Li modifications of NFs decreased the values of J_{SC} notably. While the decrease was already observed for the DSSCs, it was more evident for the PSCs. Despite the Li-TFSI treatment being widely employed in the field of PSCs to improve electron transport within the mesoporous TiO$_2$ by inducing a partial reduction of Ti^{4+} to Ti^{3+} which is associated with oxygen vacancies,[5] our results show that the

method of modification that was employed herein has the opposite effect. The direct addition of Li salt to the sol gel solution that is used for the electrospinning of TiO_2 NFs results in the TiO_2 crystal structure that is unfavorable for the charge transport. Furthermore, as discussed above no oxygen vacancies are induced which was verified with XPS and Raman spectroscopy. Contradictorily, V_{OC} increased after Li modifications on average to 41.6 mV (Table S6). Such a trend, which was also observed in our DSSCs is well known for the Li-TFSI treatment and is in agreement with the work of Giordano et al.[5] On the other hand, FF decreased and was the lowest among all for the Li modified PSCs which is in agreement with the trends of the R_S shown in Table S7. Since the latter devices exhibited the lowest J_{SC} values, the phenomenon can also be attributed to the significant increase in the R_S.

Table 3. Photovoltaic parameters for the highest performing PSC devices.

Device	J_{SC} (mA cm^{-2})	V_{OC} (mV)	FF (%)	PCE (%)
Control	19.8	839.0	51.2	8.5
La modified	21.9	871.7	60.2	11.5
Li modified	17.4	865.3	55.8	8.4

Conclusion

In summary, we demonstrated a one-step modification method for TiO_2 NFs *via* the addition of La and Li metal salts. The modifications can be accomplished with a simple addition of the metal salts directly into the precursor solution for electrospinning. It was determined that neither La or Li elements caused any considerable interstitial or substitutional doping of TiO_2 due to the large difference in ionic radius compared to Ti^{4+}. Moreover, the Li modification of TiO_2 NFs facilitated the formation of the rutile phase which

normally occurs at elevated temperatures. Therefore, the latter phase was detected by XRD together with the anatase phase. While the modification with La decreased the crystallite sizes of TiO_2 NFs, the addition of Li increased them. Such trends resulted in different BET surface areas where the La modified TiO_2 NFs exhibited the highest. It was shown that the addition of metal salts influenced the band gap values of TiO_2, specifically Li modifications were responsible for the lowest value. Lastly, TiO_2 NFs were used for a device fabrication of DSSCs and PSCs. Based on the J-V curves it was determined that the addition of La had a favourable influence on their performance characteristics. Particularly, all photovoltaic parameters increased significantly for PSCs while for DSSCs the increase in V_{OC} was not so distinguished.

Supporting Information

TEM, XPS, Raman Spectroscopy, and resistance measurement data (extracted from the *J-V* curves) has been including in the SI along with additional materials characterization information.

Author Information

Corresponding Author

* Dr. Thomas J. Macdonald, E-Mail: tom.macdonald@ucl.ac.uk

Author Contributions

References

(1) Liu, X.; Iocozzia, J.; Wang, Y.; Cui, X.; Chen, Y.; Zhao, S.; Li, Z.; Lin, Z. Noble Metal–Metal Oxide Nanohybrids with Tailored Nanostructures for Efficient Solar Energy Conversion, Photocatalysis and Environmental Remediation. *Energy Environ. Sci.* **2017**, *10* (2), 402–434. https://doi.org/10.1039/C6EE02265K.

(2) Hussain, H.; Tocci, G.; Woolcot, T.; Torrelles, X.; Pang, C. L.; Humphrey, D. S.; Yim, C. M.; Grinter, D. C.; Cabailh, G.; Bikondoa, O.; et al. Structure of a Model TiO_2 Photocatalytic Interface. *Nat. Mater.* **2017**, *16* (4), 461–466. https://doi.org/10.1038/nmat4793.

(3)   Lu, Y.; Sathasivam, S.; Song, J.; Crick, C. R.; Carmalt, C. J.; Parkin, I. P. Robust Self-Cleaning Surfaces That Function When Exposed to Either Air or Oil. *Science* **2015**, *347* (6226), 1132–1135. https://doi.org/10.1126/science.aaa0946.

(4)   Ambroz, F.; Macdonald, T. J.; Nann, T. Trends in Aluminium-Based Intercalation Batteries. *Adv. Energy Mater.* **2017**, *7* (15), 1602093. https://doi.org/10.1002/aenm.201602093.

(5)   Giordano, F.; Abate, A.; Baena, J. P. C.; Saliba, M.; Matsui, T.; Im, S. H.; Zakeeruddin, S. M.; Nazeeruddin, M. K.; Hagfeldt, A.; Graetzel, M. Enhanced Electronic Properties in Mesoporous TiO₂ via Lithium Doping for High-Efficiency Perovskite Solar Cells. *Nat. Commun.* **2016**, *7*, 10379. https://doi.org/10.1038/ncomms10379.

(6)   Alotaibi, A. M.; Sathasivam, S.; Williamson, B. A. D.; Kafizas, A.; Sotelo-Vazquez, C.; Taylor, A.; Scanlon, D. O.; Parkin, I. P. Chemical Vapor Deposition of Photocatalytically Active Pure Brookite TiO2 Thin Films. *Chem. Mater.* **2018**, *30* (4), 1353–1361. https://doi.org/10.1021/acs.chemmater.7b04944.

(7)   Roose, B.; Pathak, S.; Steiner, U. Doping of TiO2 for Sensitized Solar Cells. *Chem. Soc. Rev.* **2015**, *44* (22), 8326–8349. https://doi.org/10.1039/C5CS00352K.

(8)   Yang, L.; Leung, W. W.-F. Application of a Bilayer TiO2 Nanofiber Photoanode for Optimization of Dye-Sensitized Solar Cells. *Adv. Mater.* **2011**, *23* (39), 4559–4562. https://doi.org/10.1002/adma.201102717.

(9)   Cavaliere, S.; Subianto, S.; Savych, I.; Jones, D. J.; Rozière, J. Electrospinning: Designed Architectures for Energy Conversion and Storage Devices. *Energy Environ. Sci.* **2011**, *4* (12), 4761–4785. https://doi.org/10.1039/C1EE02201F.

(10) Fan, K.; Yu, J.; Ho, W. Improving Photoanodes to Obtain Highly Efficient Dye-Sensitized Solar Cells: A Brief Review. *Mater. Horiz.* **2017**, *4* (3), 319–344. https://doi.org/10.1039/C6MH00511J.

(11) Macdonald, T. J.; Tune, D. D.; Dewi, M. R.; Gibson, C. T.; Shapter, J. G.; Nann, T. A TiO2 Nanofiber–Carbon Nanotube-Composite Photoanode for Improved Efficiency in Dye-Sensitized Solar Cells. *ChemSusChem* **2015**, *8* (20), 3396–3400. https://doi.org/10.1002/cssc.201500945.

(12) Liqiang, J.; Xiaojun, S.; Baifu, X.; Baiqi, W.; Weimin, C.; Honggang, F. The Preparation and Characterization of La Doped TiO2 Nanoparticles and Their Photocatalytic Activity. *J. Solid State Chem.* **2004**, *177* (10), 3375–3382. https://doi.org/10.1016/j.jssc.2004.05.064.

(13) Zhang, J.; Zhao, Z.; Wang, X.; Yu, T.; Guan, J.; Yu, Z.; Li, Z.; Zou, Z. Increasing the Oxygen Vacancy Density on the TiO2 Surface by La-Doping for Dye-Sensitized Solar Cells. *J. Phys. Chem. C* **2010**, *114* (43), 18396–18400. https://doi.org/10.1021/jp106648c.

(14) Dharani, S.; Mulmudi, H. K.; Yantara, N.; Trang, P. T. T.; Park, N. G.; Graetzel, M.; Mhaisalkar, S.; Mathews, N.; Boix, P. P. High Efficiency Electrospun TiO2 Nanofiber Based Hybrid Organic–Inorganic Perovskite Solar Cell. *Nanoscale* **2014**, *6* (3), 1675–1679. https://doi.org/10.1039/C3NR04857H.

(15) Xiao, Y.; Han, G.; Li, Y.; Li, M.; Wu, J. Electrospun Lead-Doped Titanium Dioxide Nanofibers and the in Situ Preparation of Perovskite-Sensitized Photoanodes for Use in High Performance Perovskite Solar Cells. *J. Mater. Chem. A* **2014**, *2* (40), 16856–16862. https://doi.org/10.1039/C4TA03658A.

(16) Mali, S. S.; Shim, C. S.; Kim, H.; Patil, P. S.; Hong, C. K. In Situ Processed Gold Nanoparticle-Embedded TiO2 Nanofibers Enabling Plasmonic Perovskite Solar Cells to

Exceed 14% Conversion Efficiency. *Nanoscale* **2016**, *8* (5), 2664–2677. https://doi.org/10.1039/C5NR07395B.

(17) Batmunkh, M.; Macdonald, T. J.; Shearer, C. J.; Bat-Erdene, M.; Wang, Y.; Biggs, M. J.; Parkin, I. P.; Nann, T.; Shapter, J. G. Carbon Nanotubes in TiO2 Nanofiber Photoelectrodes for High-Performance Perovskite Solar Cells. *Adv. Sci.* **2017**, *4* (4), 1600504. https://doi.org/10.1002/advs.201600504.

(18) Macdonald, T. J.; Tune, D. D.; Dewi, M. R.; Gibson, C. T.; Shapter, J. G.; Nann, T. A TiO2 Nanofiber–Carbon Nanotube-Composite Photoanode for Improved Efficiency in Dye-Sensitized Solar Cells. *ChemSusChem* **2015**, *8* (20), 3396–3400. https://doi.org/10.1002/cssc.201500945.

(19) Macdonald, T. J.; Ambroz, F.; Batmunkh, M.; Li, Y.; Kim, D.; Contini, C.; Poduval, R.; Liu, H.; Shapter, J. G.; Papakonstantinou, I.; et al. TiO2 Nanofiber Photoelectrochemical Cells Loaded with Sub-12 Nm AuNPs: Size Dependent Performance Evaluation. *Mater. Today Energy* **2018**, *9*, 254–263. https://doi.org/10.1016/j.mtener.2018.06.005.

(20) Ahn, N.; Son, D.-Y.; Jang, I.-H.; Kang, S. M.; Choi, M.; Park, N.-G. Highly Reproducible Perovskite Solar Cells with Average Efficiency of 18.3% and Best Efficiency of 19.7% Fabricated via Lewis Base Adduct of Lead(II) Iodide. *J. Am. Chem. Soc.* **2015**, *137* (27), 8696–8699. https://doi.org/10.1021/jacs.5b04930.

(21) Ma, Y.-T.; Li, S.-D. Photocatalytic Activity of TiO2 Nanofibers with Doped La Prepared by Electrospinning Method. *J. Chin. Chem. Soc.* **2015**, *62* (4), 380–384. https://doi.org/10.1002/jccs.201400243.

(22) HORN, M.; SCHWEBDTFEGER, C. F.; MEAGHER, E. P. Refinement of the Structure of Anatase at Several Temperatures. *Z. Für Krist. - Cryst. Mater.* **1972**, *136* (1–6), 273–281. https://doi.org/10.1524/zkri.1972.136.16.273.

(23) Tanyi, A. R.; Rafieh, A. I.; Ekaneyaka, P.; Tan, A. L.; Young, D. J.; Zheng, Z.; Chellappan, V.; Subramanian, G. S.; Chandrakanthi, R. L. N. Enhanced Efficiency of Dye-Sensitized Solar Cells Based on Mg and La Co-Doped TiO2 Photoanodes. *Electrochimica Acta* **2015**, *178*, 240–248. https://doi.org/10.1016/j.electacta.2015.07.172.

(24) Priyanka, K. P.; Revathy, V. R.; Rosmin, P.; Thrivedu, B.; Elsa, K. M.; Nimmymol, J.; Balakrishna, K. M.; Varghese, T. Influence of La Doping on Structural and Optical Properties of TiO2 Nanocrystals. *Mater. Charact.* **2016**, *113*, 144–151. https://doi.org/10.1016/j.matchar.2016.01.015.

(25) Ambroz, F.; Macdonald, T. J.; Martis, V.; Parkin, I. P. Evaluation of the BET Theory for the Characterization of Meso and Microporous MOFs. *Small Methods* **2018**, *0* (0), 1800173. https://doi.org/10.1002/smtd.201800173.

(26) Subramanian, A.; Bow, J.-S.; Wang, H.-W. The Effect of Li+ Intercalation on Different Sized TiO2 Nanoparticles and the Performance of Dye-Sensitized Solar Cells. *Thin Solid Films* **2012**, *520* (23), 7011–7017. https://doi.org/10.1016/j.tsf.2012.07.055.

(27) Li, H.; Zheng, B.; Xue, Y.; Liu, S.; Gao, C.; Liu, X. Spray Deposited Lanthanum Doped TiO2 Compact Layers as Electron Selective Contact for Perovskite Solar Cells. *Sol. Energy Mater. Sol. Cells* **2017**, *168*, 85–90. https://doi.org/10.1016/j.solmat.2017.04.027.